Nov 13th, 12:00 AM

Distortional Buckling of Steel Storage Rack Columns

Gregory J. Hancock

Seventh International Specialty Conference on Cold-Formed Steel Structures
St. Louis, Missouri, U.S.A., November 13-14, 1984

DISTORTIONAL BUCKLING OF STEEL STORAGE RACK COLUMNS

Gregory J. Hancock*

Summary

A distortional mode of buckling is described for cold-formed lipped channel columns which have additional flanges attached to the flange stiffening lips. The purpose of the additional flanges (called 'rear flanges') is to permit bolting of braces to the channel section so as to form upright frames of steel storage racks.

Theoretical and experimental evidence of this mode of buckling is provided for perforated and unperforated columns. A set of design charts is included to permit calculation of the distortional buckling stresses of a range of sizes of practical channel sections with rear flanges.

* Senior Lecturer, School of Civil and Mining Engineering, University of Sydney, N.S.W., Australia, 2006.

1. INTRODUCTION

The columns of industrial steel storage racks are generally cold-formed lipped channels. They are braced into upright frames by connecting inclined or horizontal bracing between the channel lips of opposing channels using either welded or bolted connections. If welding is used, the braces are welded directly to the flange stiffening lips as shown in Fig.1(a). Consequently a conventional lipped channel can be used as the column profile in a welded system. However, if bolting is used, additional elements parallel with the channel flanges and located at the ends of the flange stiffening lips, as shown in Fig. 1(b), are often used to permit the braces to be bolted to the channel column. These additional elements (called 'rear flanges') are often wide and may require additional lip stiffeners as shown in Fig.1(b). The alternative bolting scheme, shown in Fig.1(c) avoids the need for rear flanges by bolting the braces directly to the front face of the channel section. However, the bolted connection produced is generally less effective in resisting flexural-torsional buckling and in-plane buckling of the braced frames than either the welded system or the bolted system which uses rear flanges. This paper describes the buckling behaviour of cold-formed column profiles with rear flanges.

The effect of the rear flanges is to destabilize the section when subjected to compression. For sections composed of thin plate, a distortional mode of buckling of the whole section can occur at a lower load than those for the local, flexural or flexural-torsional buckling modes. The distortional mode occurs at a significantly longer wavelength than the local buckling mode and cannot be detected in a conventional stub column test. In addition, distortional effects may also lower the flexural-torsional buckling load.

The finite strip method of buckling analysis developed by Przmieniecki (Ref.9) and Plank and Wittrick (Ref.8) has been used to investigate the local, distortional and flexural-torsional modes of buckling of I-beams (Ref.4), lipped channels used as purlins (Ref.5), lipped channels used as framing members in portal frames (Ref.2), and unlipped channels used as compression members (Ref.6). In Section 2 of this paper, the method is used to investigate the different modes of buckling, particularly the distortional mode, of cold-formed channel columns with rear flanges. A set of design charts, giving the distortional buckling stresses of columns of this type, is included in Section 4 of the paper.

Compression tests of a roll-formed commercial profile are described in Section 3. The sections were tested both with and without perforations (slots) and in two different plate thicknesses. The test failure stresses are compared with the theoretical distortional buckling stresses. Unlike local buckling, the distortional buckling mode does not appear to have a significant post-buckling reserve of strength before material yielding causes failure.

2. BUCKLING MODES OF CHANNELS IN COMPRESSION

2.1 Sections Studied

Three different section geometries have been chosen for analysis to demonstrate the different modes of buckling of lipped channels with rear flanges. The basic profile (Section 1) in Fig.2(a) is a lipped channel with sloping lip stiffeners. Sloping lip stiffeners were chosen so that Section 2 (shown in Fig.2(b)) is identical with Section 1 except for the inclusion of the rear flanges. The geometry of Section 2 has been chosen to be representative of a typical channel with rear flanges. Section 3 (shown in Fig.2(c)) is identical with Section 2 except for the inclusion of additional lip stiffeners on the rear flanges. All three sections studied were of the same overall depth of 3.15 in. (80 mm) and plate thickness 0.059 in.(1.5 mm).

2.2 Finite Strip Model

The finite strip method involves subdividing the channel section into longitudinal strips as shown in Fig.3. Each strip is assumed to be free to deform both in its plane (membrane displacements) and out of its plane (flexural displacements) in single half sine waves over the length of the section being analysed. The ends of the section under study are assumed free to deform longitudinally but are prevented from deforming in a cross-sectional plane. The buckling modes computed are for a single buckle half-wavelength. Details of the analytical method and its application to cases where multiple half-wavelengths occur within the length of a column under study are given in Ref.4.

In the case of flexural-torsional buckling, the boundary conditions used in the finite strip analysis are identical with those used by Timoshenko and Gere (Ref.10) for a simply supported column free to warp at its ends and buckling in a single half-wavelength over the column length. The actual columns in storage racks are not restrained by such simple supports and different effective lengths for flexure and torsion frequently occur. In addition, section distortion at the support points may occur and the simple assumptions of both the finite strip method and Timoshenko theory are invalidated. A program of testing and theoretical work to investigate the effect of section distortion on flexural-torsional buckling is currently underway at the University of Sydney.

For the modes of local and distortional buckling, multiple half-wavelengths generally occur within the regions between supports. Hence the end boundary conditions of column lengths of actual rack columns have very little effect on the buckling loads of the local and distortional modes and the results of the finite strip analysis provide accurate predictions of section buckling loads.

For the channel section shown in Fig.3, each flat element, other than the lip stiffeners, has been subdivided

into two elements. This subdivision was shown in Ref.8 to produce an error less than 1% for thin-walled sections assumed subjected to uniform compression. The subdivision results in 12 strips separated by 13 nodal lines for section 2 in Fig.3. Since the analysis uses 4 degrees of freedom per nodal line, the folded plate system has 52 degrees of freedom. All buckling calculations were performed on a SIRIUS I (16 bit) microcomputer using eigenvalue and eigenvector routines specifically developed for the purpose (Ref.7).

2.3 Section 1

The results of a stability analysis of Section 1, subjected to uniform compression, are shown in Fig.4, which represents the buckling load versus half-wavelength of the buckle. A minimum (Point A) occurs in the curve at a half-wavelength of 65 mm and represents local buckling in the mode shown in Fig.4. The local mode mainly consists of deformation of the front face plate element. The elastic critical stress for local buckling of the front face element alone is given (Ref.10) by

$$F_l = \frac{K_l \pi^2 E}{12(1-\nu^2)} / (D/t)^2 \qquad (1)$$

where K_l is equal to 4.0 for a simply supported plate. The critical stress determined using equation (1) is shown in Fig. 4 and is lower than the finite strip value since the finite strip value includes the restraints to the edges of the front face provided by the flanges.

A minimum occurs at point B at a half-wavelength of 11.0 in (280 mm) in the mode shown in Fig. 4. This mode involves mainly a rigid body rotation of the flange and lip combinations about the junction of the flanges and front face, with the front face element restraining the flanges. This mode is called a DISTORTIONAL buckling mode in this paper. In some reports, it has been called a stiffener buckling mode since it involves membrane buckling of the stiffener. However, the term stiffener buckling has also been used in other reports to describe local buckling of the stiffener alone and confusion can occur with this terminology.

The distortional buckling stress at point B is slightly higher than the local buckling stress at point A, so that when the section is subjected to compression, it is likely to undergo local buckling in preference to distortional buckling. A detailed discussion of local and distortional buckling of lipped channels in compression, including tests, is given in Ref.3.

At long half-wavelengths, such as at points C, D and E in Fig. 4, the section buckles in a flexural or flexural-torsional buckling mode. For this particular

geometry section, flexural-torsional buckling occurs at half-wavelengths up to approximately 70 in. (1800 mm) beyond which flexural buckling occurs. In the range 30-70 in (800-1800 mm), the graph through C, D on Fig. 4 agrees almost identically (see Table 1) with values predicted using the Timoshenko formula (Ref.10) for flexural-torsional buckling. At longer half-wavelengths, the graph through E agrees almost identically with the Euler formula for flexural buckling of a column.

2.4 Section 2

The results of a stability analysis of Section 2, subjected to uniform compression, are shown in Fig. 5. This graph is similar in form to that drawn in Fig. 4. However, the destabilizing influence of the additional rear flanges has lowered the distortional buckling stress from 54.4 ksi (375 MPa) for Section 1 to 26.1 ksi (180 MPa) for Section 2. The half-wavelength of the distortional buckle has been increased to 13.8 in. (350 mm) for Section 2 from 11.0 in. (280 mm) for Section 1. The value of distortional buckling stress for Section 2 is sufficiently low that distortional buckling will occur before flexural-torsional buckling when the column restraints limit the buckle half-wavelength of the flexural-torsional mode to less than 55 in. (1400 mm). Hence the distortional buckling mode becomes a serious consideration in the design of such a column.

A test of a short length column between rigid end plattens would require that the specimen length be at least twice the distortional buckle half-wavelength (i.e 2 x 13.8 = 27.6 in. (700 mm)), since the distortional buckling mode involves membrane buckling of the lip stiffeners. A conventional stub column test, as specified in the Rack Manufacturer's Institute Specification (Ref.11) for determination of the Q-factor, is generally performed on a specimen which is much shorter than twice the distortional buckle half-wavelength. Hence the distortional buckling mode is unlikely to be detected in a conventional stub column test.

The local buckling stress at A in Fig. 5 is almost identical with that at A in Fig. 4, since the local buckling mode is confined mainly to the front face and is not affected by the rear flanges. The local buckling stress of the rear flange alone, treated as an unstiffened element with K_1 equal to 0.50, is also shown in Fig. 5. However, the elastic restraint provided to the rear flanges by the flange lips has apparently eliminated this mode of local buckling of the rear flanges of Section 2.

The flexural-torsional buckling mode occurs at a half-wavelength of 55 in. (1400 mm) and above. The finite strip value at 59 in. (1500 mm) (point D in Fig. 5) is 2 4% lower than the Timoshenko formula (Ref.10) as a consequence of slight section distortions in the flexural-torsional mode. The value of the flexural-torsional buckling stress, computed for Section 2 at a half-wavelength of 59 in. (1500 mm) (Point D in Fig.5) is 12.9%

higher (see Table 1) than that for Section 1 at the same half-wavelength (Point D in Fig.4). Obviously the section with the rear flanges is more efficient at resisting flexural-torsional buckling, probably as a result of a fourfold increase in the section warping constant (see Table 2).

2.5 Section 3

The results of a stability analysis of Section 3, subjected to uniform compression, are shown in Fig. 6. This graph is also similar in form to that drawn in Figs. 4 and 5. However, the destabilizing influence of the rear flanges has been significantly decreased by the inclusion of the additional stiffening lips on the rear flanges. The distortional buckling stress at point B has been increased from 26.1 ksi (180 MPa) for Section 2 in Fig. 5 to 39.2 ksi (270 MPa) for Section 3 in Fig. 6. Distortional buckling will only control the design of Section 3 when the column restraints limit the buckle half-wavelength of the flexural-torsional mode to less than 40 in. (1000 mm). Hence the distortional buckling mode will be a much less serious consideration in the design of a column with additional lip stiffeners than it would be for the section with unstiffened rear flanges.

Unfortunately, inclusion of the additional lip stiffeners results in two adverse consequences affecting the flexural-torsional buckling strength of the section. Firstly, as shown in Fig. 6, the effect of section distortion reduces the flexural-torsional buckling stress at a half-wavelength of 59 in (1500 mm) (Point D) by 4.2% below the classical flexural-torsional buckling stress. Secondly, the additional lip stiffeners cause the shear centre to move further from the centroid of the section (see Table 2) with a consequent reduction in the classical flexural-torsional buckling stress of Section 3 by 13.1% (see Table 1) below that for Section 2 without the additional lip stiffeners. Allowing for the effects of distortion on both sections, Section 3 buckles in a flexural-torsional mode at a half-wavelength of 59 in. (1500 mm) at a stress which is 14.9% lower than that for Section 2. Hence the inclusion of the additional lip stiffeners will be detrimental to the strength of the section where flexural-torsional buckling controls the design.

3. TESTS

3.1 General

A series of tests was undertaken at the University of Sydney for Colby Engineering Pty. Ltd. of Sydney, Australia. The tests were performed on a commercial profile (named C0001) shown in Fig. 7. The section is similar to that represented by Section 2 in Fig.2(b), except for the intermediate stiffener in the front face and the inclusion of slots in both the front face and rear flanges.

Tests were performed on three different section lengths to investigate local, distortional and flexural-torsional buckling. The stub column tests to investigate local buckling were carried out between rigid plattens on 11.8 in. (300 mm) long specimens. The tests to investigate distortional buckling were also performed between rigid plattens on 35.4 in. (900 mm) long specimens and those to investigate flexural-torsional buckling were performed between centroidally located ball seats on 102 in. (2590 mm) long specimens with torsional braces at 47.2 in. (1200 mm) centres. The complete set of test results is described in Ref.12 and only the results of the distortional buckling tests are described in detail in this paper.

As part of the investigation work in preparing this paper, additional distortional buckling tests were performed on the same profile in Fig. 7 but without slots. The objective of the latter tests was to determine whether the distortional buckling stresses described in Ref. 12 had been influenced by the slots.

3.2 Distortional Buckling Tests

The distortional buckling test specimens were prepared in accordance with the stub column test procedure of Ref. 11. The length of the specimens was chosen to be 35.4 in. (900 mm) which is twice the distortional buckle half-wavelength of 17.7 in (450 mm). The length was chosen as twice the distortional buckle half-wavelength, since the distortional buckling mode involves in-plane bending of the lip stiffeners which would be held fixed by the rigid end plattens. Consequently the effective length for buckling of the lip stiffeners would be half of the test specimen length and thus equal to the distortional buckle half-wavelength. The resulting specimen length, which is 41.6 times the least radius of gyration, is more than double that normally permitted for a stub column test in the AISI specification (Ref. 1).

The measured dimensions of the test specimens are given in Table 3 for the section in Fig.7. Specimens D1, D2 were those without slots and specimens D3-D6 included slots. Specimens D1-D4 were of nominal plate thickness 0.063 in.(1.6 mm) and D5,D6 were of nominal plate thickness 0.079 in. (2.0 mm) material. The high tensile steel from which the specimens were roll-formed was found to have no sharply defined yield point and so the 0.2% proof stress was taken as the yield point. The 0.2% proof stresses of the 0.063 in. (1.6 mm) and 0.079 in. (2.0 mm) thick materials were 75.9 ksi (523 MPa) and 70.6 ksi (487 MPa) respectively.

When the roll-formed sections were cut into 35.4 in. (900 mm) lengths for testing, the open profile sprang apart slightly at each end. The increase in the distance between the tips of the rear flanges, resulting from springing, varied between 0.2 - 0.4 in. (5-10 mm) approximately.

The specimens were tested in compression in an Instron TT-KM (25 tonne) testing machine under displacement control to determine their maximum load capacity. A calibrated extensometer was located between the tips of the rear flanges at the centre of each specimen to measure deformation of the distortional mode of buckling during loading. The load-deformation graph, taken from the extensometer located between the flange tips of specimen D1, is shown in Fig. 8. Initially the flange tips moved inwards, as a consequence of the initial imperfection created by the outward springing at the ends of the sections. However, as the load was increased, the specimen developed distortional buckles of approximately the same half-wavelength as those computed theoretically, and the flange tips moved outwards at the centre as shown in Fig. 8. Fig. 9 shows the buckled mode at a load of approximately 21.4 kip (95 kN). The long-wavelength distortional buckle is clearly visible. At a load of 22.7 kip (100.8 kN), the flange tips had moved outwards by approximately 0.4 in (10 mm) and yielding resulted in failure of the section. Continued compression of the specimen produced a gradual unloading with no sudden fall in load capacity.

3.3 Failure Stress

The maximum load and average stress attained by each specimen has been computed in Table 4 based on the maximum load divided by the nett cross-sectional area. The nett cross-sectional area has been taken as the product of the plate thickness with the difference of the strip width minus the maximum total slot width. The slots in the rear flanges and front face were slightly staggered so that the maximum slot width was not simply the sum of the full width of all the slots.

The four specimens D1-D4 in nominal 0.063 in. (1.6 mm) material failed at an average stress of 35.1 ksi (242 MPa). This stress is slightly higher than the theoretical distortional buckling stress of an unperforated section of 34.2 ksi (236 MPa) computed using a finite strip model of the C0001 section including the intermediate stiffener in the front face. There is no significant difference between the values for the perforated and unperforated sections when the nett cross-sectional area is used. The two specimens D5, D6 of nominal 0.079 in. (2.0 mm) material failed at an average stress of 41.6 ksi (287 MPa) which is 9% less than the theoretical distortional buckling stress of an unperforated section computed using the finite strip analysis.

The stub column strengths, taken from Ref.12, were 45.4 ksi (313 MPa) and 46.4 ksi (320 MPa) for specimens roll-formed from 0.063 in. (1.6 mm) and 0.079 in. (2.0 mm) thick material. Hence for the 0.063 in. (1.6 mm) thick sections, the theoretical distortional buckling stress is 75% of the stub column strength and so the distortional buckling test specimens reached the distortional buckling stress before significant yielding occurred. However, for

the 0.079 in. (2.0 mm) thick section, the theoretical distortional buckling stress is 98% of the stub column strength and so the two phenomena interact to produce a distortional buckling test strength which is 91% of the theoretical distortional buckling strength.

3.4 Interaction of Flexural-Torsional and Distortional Buckling

Different modes of buckling, which have almost coincident buckling loads, have been shown to interact adversely in some instances (Ref. 13) and therefore should be investigated. Consequently the test results, described in Ref.12, were studied to see if there was evidence of adverse interaction of distortional and flexural-torsional buckling.

In one of the flexural-torsional buckling tests, a flexural-torsional buckling mode was found to occur at a load slightly below that for distortional buckling. In this test, the distortional buckle waves were observed to develop in the rear flanges before flexural-torsional buckling occurred. However, there was no adverse interaction and the specimen failed at a similar load to what would have occurred if no distortional buckles had developed.

4. DESIGN CHARTS FOR DISTORTIONAL BUCKLING

Designers do not generally have access to a finite strip computer analysis, and so a simplified procedure for calculating the distortional buckling stress is required. The procedure presented in this paper is to provide graphs of non-dimensional buckling coefficients for use with the local buckling equation (1). A confirmation of this procedure was provided by performing an analysis of Section 2 in Fig. 2 with all dimensions, including thickness, reduced by one half. The analysis produced exactly the same distortional buckling stress at precisely half the previously computed buckling half-wavelength.

The distortional mode of buckling involves membrane deformation of the lip stiffeners, and so the buckling coefficient is not independent of plate thickness as it would be for a purely local buckle. Hence the graphs of buckling coefficient have been prepared as a function of the non-dimensional plate slenderness of the front face (D/t). The buckling coefficients were computed from the results of finite strip analyses using

$$K_d = F_d \left[\frac{12(1-\nu^2)}{\pi^2 E}\right]\left(\frac{B^*}{t}\right)^2 \qquad (2)$$

where F_d is the distortional buckling stress and B* is the overall section width including the rear flanges and lip stiffeners, as shown in Fig. 10.

The graphs have been prepared for a section in which the flange lip stiffeners are located midway across

the overall flange widths and inclined at an angle of 45 degrees to the flanges. It is normal in these types of sections for the lip to be inclined and 45 degrees was chosen as being reasonably representative. To investigate the effect of varying the angle of the lip stiffener, an analysis was performed on Section 2 in Fig. 2, but with the lip stiffener perpendicular to the flanges and with the total flange width (B* = 2.76 in. (70 mm)) kept constant. For this section, the distortional buckling stress increased by approximately 11 percent from 26.1 ksi (180 MPa) for Section 2 (Table 1) to 29.0 ksi (200 MPa). Hence the design charts, calculated for a section with a 45 degree lip stiffener, will produce a lower bound, provided that the angle the lip stiffener makes with the flanges is greater than 45 degrees.

The graphs have been prepared for a lip stiffener dimensions (L) as a fraction of the section depth (D) ranging from 0.10 to 0.25. For sections with lip stiffeners less than approximately 0.10D, only one minimum point occurs on the graph of buckling stress versus half-wavelength. For the particular case of no lip stiffener (L/D = 0.0), the buckling mode is purely local and the buckling coefficient for the flange is independent of the plate slenderness (D/t).

Two design charts have been prepared at values of B*/D equal to 0.70 and 0.90, which cover the main range of application of sections of this type. They are shown in Figs. 11 and 12 where the upper graph gives the buckling coefficient (K_d) and the lower graph gives the half-wavelength (λ_d) of the distortional buckle. Note that the values of K_d and λ_d vary with plate slenderness (D/t) except for the particular case of no lip stiffener (L/D = 0.0) where local buckling predominates. For valuesof B*/D between 0.70 and 0.90, linear interpolation based on the values taken from each chart can be used with an accuracy better than 2 percent.

The primary local buckling minimum (point A in Fig. 5) was computed for all of the sections used to prepare the distortional buckling charts in Figs. 11 and 12. Except for the cases where L/D was less than 0.10, and no primary local minimum occurred in the graphs of buckling stress versus half-wavelength, the local buckling coefficient K_l, based on the slenderness of the front face (D/t), was always in the range 5.5 to 5.85. The primary local buckling minimum (point A in Fig. 5) was always higher than the distortional buckling minimum (point B in Fig. 5) and so distortional buckling always controlled in preference to local buckling.

Designers should make an allowance for realistic imperfections when using the design charts for practical use. These include eccentric loading, unbalanced end conditions, out-of-plumbness and other field situations.

5. CONCLUSIONS

A distortional mode of buckling has been described for cold-formed lipped channel sections with rear flanges attached to the flange stiffening lips. The purpose of the rear flanges is to allow braces to be bolted to cold-formed channel section columns.

Both theoretical and experimental evidence of the distortional mode of buckling has been presented, and it has been shown experimentally that there is very little post buckling strength available for this mode of buckling. It has also been demonstrated, for a particular commercial profile, that the failure stresses of a perforated and an unperforated section, in the distortional mode, are similar when the stresses are based on the nett section area.

A set of design charts, for sections with rear flanges, has been provided to enable calculation of the distortional buckling stresses and buckling half-wavelengths of a range of section geometries. For all of the sections investigated, distortional buckling occurred at a lower stress than local buckling. It has also been demonstrated that the inclusion of additional stiffening lips on the rear flanges, to raise the distortional buckling stress, may lower the flexural-torsional buckling stress and thus make the section less efficient.

6. REFERENCES

1. American Iron and Steel Institute, Specification for the Design of Cold-Formed Steel Structural Members, Washington, DC (1980).

2. Baigent, A.H. and Hancock, G.J., "The Strength of Cold-Formed Portal Frames", Proceedings, Sixth International Speciality Conference on Cold-Formed Steel Structures, St. Louis, Missouri, November, 1982.

3. Desmond, T.P., Pekoz, T., and Winter, G., "Edge Stiffeners for Thin-Walled Members", Journal of the Structural Division, ASCE, Vol. 107, No. ST2, Feb. 1981, pp 329-352.

4. Hancock, G.J., "Local, Distortional and Lateral Buckling of I-Beams", Journal of the Structural Division, ASCE, Vol. 104, No. ST 11, Nov. 1978, pp 1787-1798.

5. Hancock, G.J., "The Behaviour and Design of Cold-Formed Purlins", Journal of the Australian Institute of Steel Construction, Vol. 15, No. 3, 1981.

6. Hancock, G.J., "The Behaviour and Design of Cold-Formed Channels in Compression", Journal of the Australian Institute of Steel Construction, Vol. 17, No. 3, 1983.

7. Hancock, G.J., "Eigenvalue Routines for Structural Buckling and Vibration Analyses on Microcomputers", 9th Australiasian Conference on the Mechanics of Structures and Materials, University of Sydney, August 1984.

8. Plank, R.J. and Wittrick, W.H., "Buckling Under Combined Loading of Thin, Flat-Walled Structures by a Complex Finite Strip Method", International Journal for Numerical Methods in Engineering, Vol. 8, No. 2, 1974, pp 323-339.

9. Przmieniecki, J.S., "Finite Element Structural Analysis of Local Instability", Journal of American Institute of Aeronautics and Astronautics, Vol.11, No. 1, Jan 1973.

10. Timoshenko, S.P. and Gere, J.M., "Theory of Elastic Stability", McGraw-Hill Book Co. Inc., New York, NY, 1959.

11. Rack Manufacturers Institute, Specification for the Design, Testing and Utilisation of Industrial Steel Storage Racks, Chicago (1979).

12. University of Sydney, School of Civil and Mining Engineering, "Tests of Column Sections of Pallet Racking", Investigation Report, No.S465, October 1983.

13. Van Der Neut, A., "The Interaction of Local Buckling and Column Failure of Thin-Walled Compression Members", Proceedings, 12th International Congress on Applied Mechanics, Springerverlag, Germany, 1969.

7. NOTATION

A	Area of cross-section
B	Flange or rear flange width (see Fig. 10)
B*	Total section width (see Fig. 10)
C_w	Section warping constant
D	Section depth (Width of front face) (See Fig. 10)
E	Young's Modulus
F_l	Local buckling stress
F_d	Distortional buckling stress
I_x, I_y	Section second moments of area about x,y axes
J	Section torsion constant

K_l Local buckling coefficient

L Lip dimension (see Fig. 10)

t Plate thickness

Distance from front face to section centroid

x_o Distance between section shear centre and centroid

ν Poisson's ratio

λ_d Half-wavelength of distortional buckle

8. ACKNOWLEDGEMENTS

The work has been carried out in the School of Civil and Mining Engineering at the University of Sydney. Calculations were performed on a SIRIUS I microcomputer provided by the University of Sydney. The tests were performed in the J.W. Roderick Structures laboratory at the University of Sydney.

The author is grateful to Colby Engineering Pty. Ltd., Brookvale, NSW, Australia for permission to use the distortional buckling test results of their proprietary sections.

TABLE 1

BUCKLING STRESSES

	UNITS	SECTION 1	SECTION 2	SECTION 3
Local Buckling Stress	ksi (MPa)	49.6 (342)	50.2 (346)	51.2 (353)
Local Buckling Half-wavelength	in (mm)	2.6 (65)	2.6 (65)	2.6 (65)
Distortional Buckling Stress	ksi (MPa)	54.4 (375)	26.1 (180)	39.2 (270)
Distortional Buckling Half-Wavelength	in (mm)	11.0 (280)	13.8 (350)	20.5 (520)
Finite Strip Flexural-Torsional Buckling Stress*	ksi (MPa)	20.7 (142.9)	23.4 (161.3)	20.3 (140.0)
Timoshenko Flexural-Torsional Buckling Stress*	ksi (MPa)	20.6 (142.0)	24.0 (165.2)	21.2 (146.0)

* Simply supported column length = 59.0 in. (1500 mm)

TABLE 2

SECTION PROPERTIES

	SECTION 1	SECTION 2	SECTION 3
A $\frac{in^2}{(mm^2)}$	0.393 (252)	0.530 (342)	0.577 (372)
$\bar{x}$ $\frac{in.}{(mm)}$	0.44 (11.2)	0.89 (22.7)	1.04 (26.5)
I_x $\frac{in^4}{(mm^4)}$	0.652 (0.260×10^6)	0.820 (0.341×10^6)	0.909 (0.378×10^6)
I_y $\frac{in^4}{(mm^4)}$	0.114 (0.0475×10^6)	0.435 (0.181×10^6)	0.584 (0.243×10^6)
J $\frac{in^4}{(mm^4)}$	0.00045 (0.189×10^3)	0.00062 (0.257×10^3)	0.00067 (0.279×10^3)
x_0 $\frac{in}{(mm)}$	1.11 (28.3)	2.14 (54.3)	2.43 (61.8)
C_w $\frac{in^6}{(mm^6)}$	0.265 (0.0712×10^9)	1.149 (0.309×10^9)	1.342 (0.361×10^9)

TABLE 3

MEASURED TEST SPECIMEN DIMENSIONS

SPECIMEN NO.	A* (mm)	B (mm)	C* (mm)	D (mm)	E* (mm)	F* (mm)	S1* (mm)	S2* (mm)	t (mm)
D1	17.2	89.6	38.5	9.5	**	31.4	**	**	1.625
D2	16.8	89.5	38.4	9.6	**	32.0	**	**	1.63
D3	15.8	87.8	37.5	10.8	12.2	33.8	14.6	11.0	1.64
D4	16.6	87.7	36.7	10.9	12.1	34.0	14.7	11.0	1.625
D5	15.7	88.8	37.5	10.9	12.2	34.4	14.6	11.0	2.01
D6	15.8	88.9	36.9	10.8	12.1	35.3	14.6	10.9	2.025

Specimen length = (35.4 in.) 900 mm

* Mean of values on each flange
** Specimens D1 and D2 unperforated
1 in. = 25.4 mm

Symbols A, B, C, D, E, F, S1, S2 and t defined in Fig.7

TABLE 4

TEST SPECIMEN FAILURE STRESSES

SPECIMEN NO.	t in (mm)	STRIP WIDTH in (mm)	GROSS AREA in^2 (mm^2)	MAX SLOTS in (mm)	NETT AREA in^2 (mm^2)	MAX LOAD kip (kN)	MAX STRESS ksi (MPa)	F_d^* ksi (MPa)
D1	0.064 (1.625)	9.69 (246)	0.620 (400)	0 (0)	0.620 (400)	22.7 (100.8)	36.5 (252)	34.2 (236)
D2	0.064 (1.63)	9.69 (246)	0.622 (401)	0 (0)	0.622 (401)	20.9 (92.9)	33.6 (232)	34.2 (236)
D3	0.064 (1.64)	9.69 (246)	0.625 (403)	1.34 (34)	0.540 (348)	18.9 (84.0)	35.1 (242)	34.2 (236)
D4	0.064 (1.625)	9.69 (246)	0.620 (400)	1.34 (34)	0.535 (345)	18.7 (83.1)	35.0 (241)	34.2 (236)
D5	0.079 (2.01)	9.69 (246)	0.766 (494)	1.34 (34)	0.660 (426)	26.9 (119.6)	40.8 (281)	45.5 (314)
D6	0.080 (2.025)	9.69 (246)	0.772 (498)	1.34 (34)	0.665 (429)	28.2 (125.4)	42.3 (292)	45.5 (314)

F_d^* = Theoretical Elastic Distortional Buckling Stress

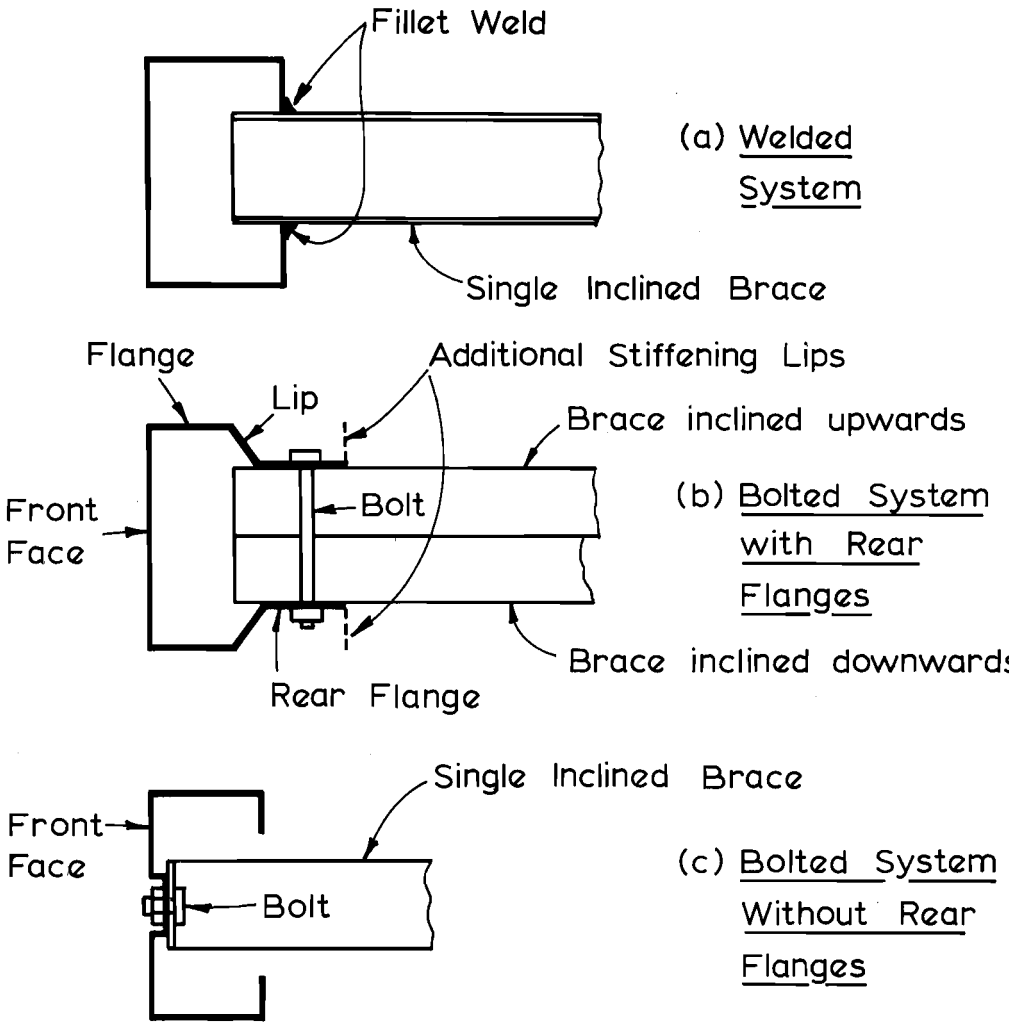

FIG. 1 UPRIGHT COLUMNS OF STEEL STORAGE RACKS

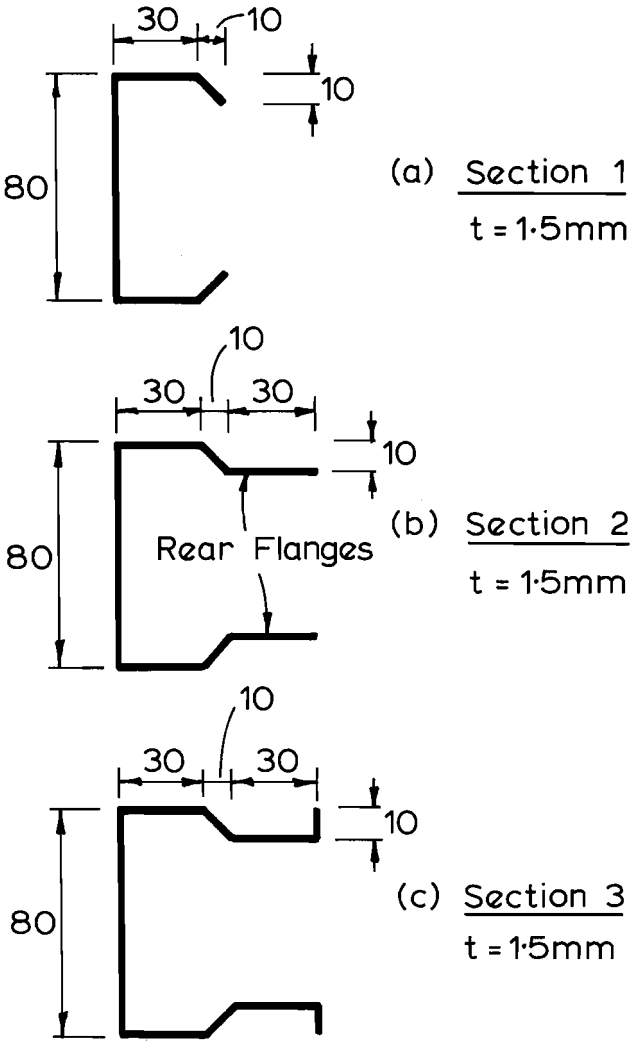

80mm = 3·15 in.
30mm = 1·18 in.
10mm = 0·39 in.
1·5mm = 0·059 in.

FIG. 2 GEOMETRY OF SECTIONS STUDIED

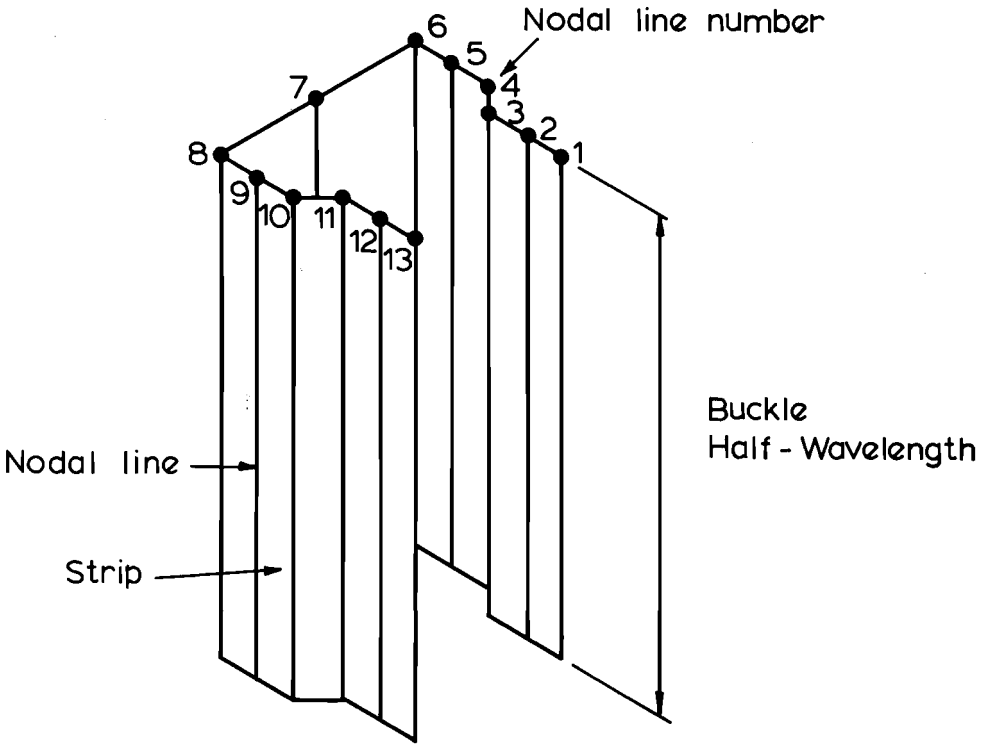

FIG. 3 FINITE STRIP MODEL (SECTION 2)

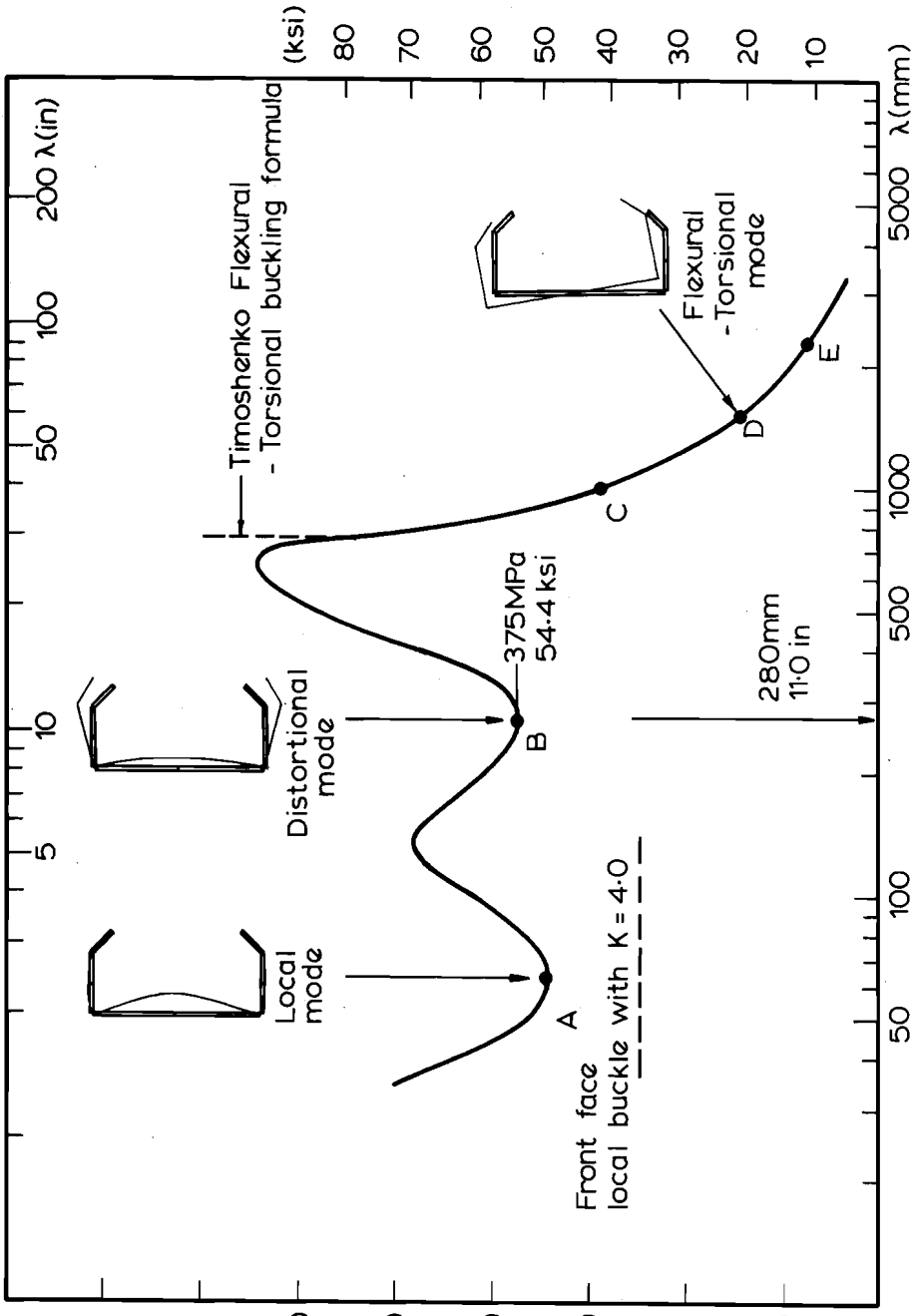

FIG. 4 SECTION 1- BUCKLING STRESS VERSUS HALF-WAVELENGTH

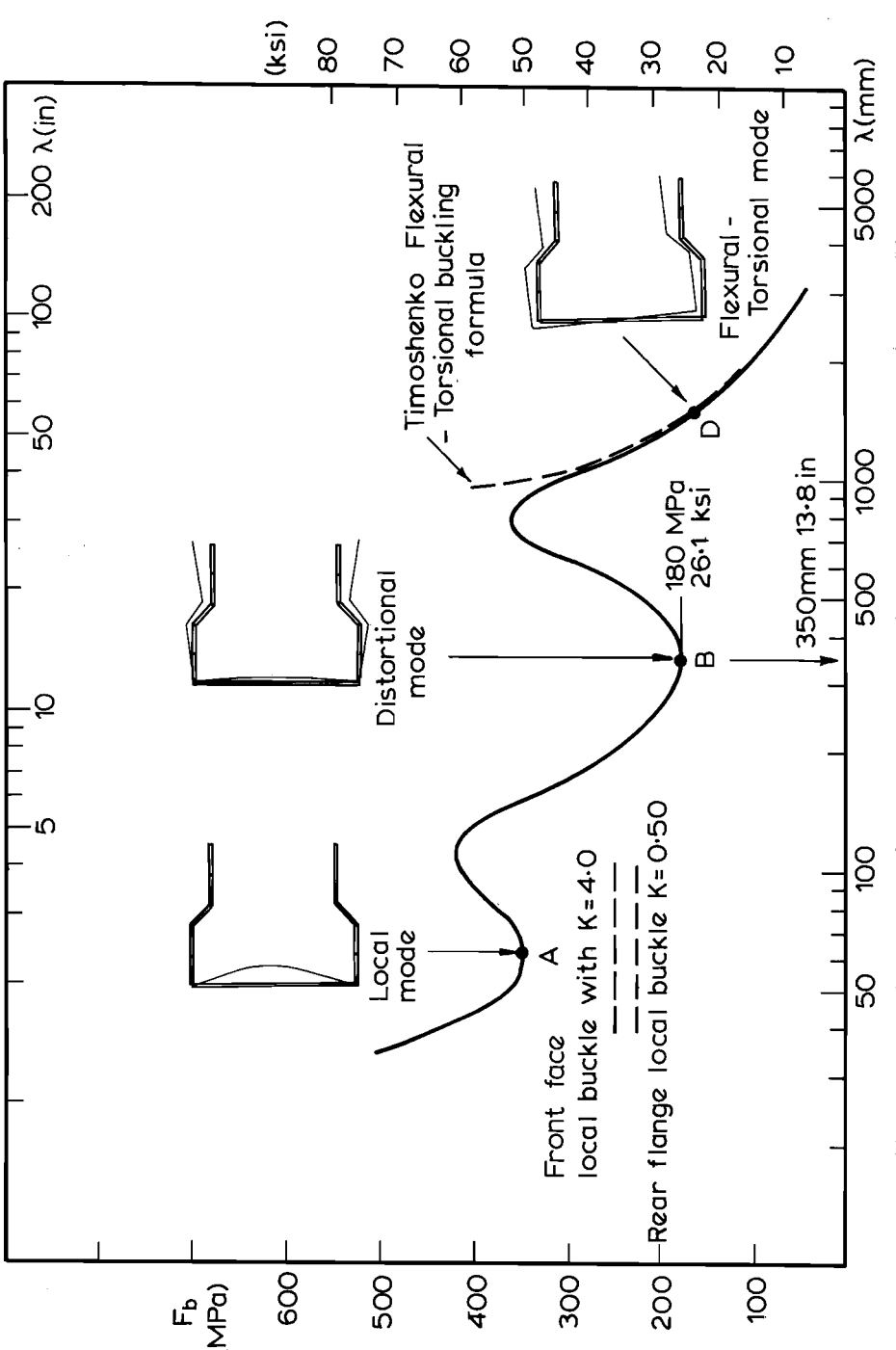

FIG. 5 SECTION 2 - BUCKLING STRESS VERSUS HALF - WAVELENGTH

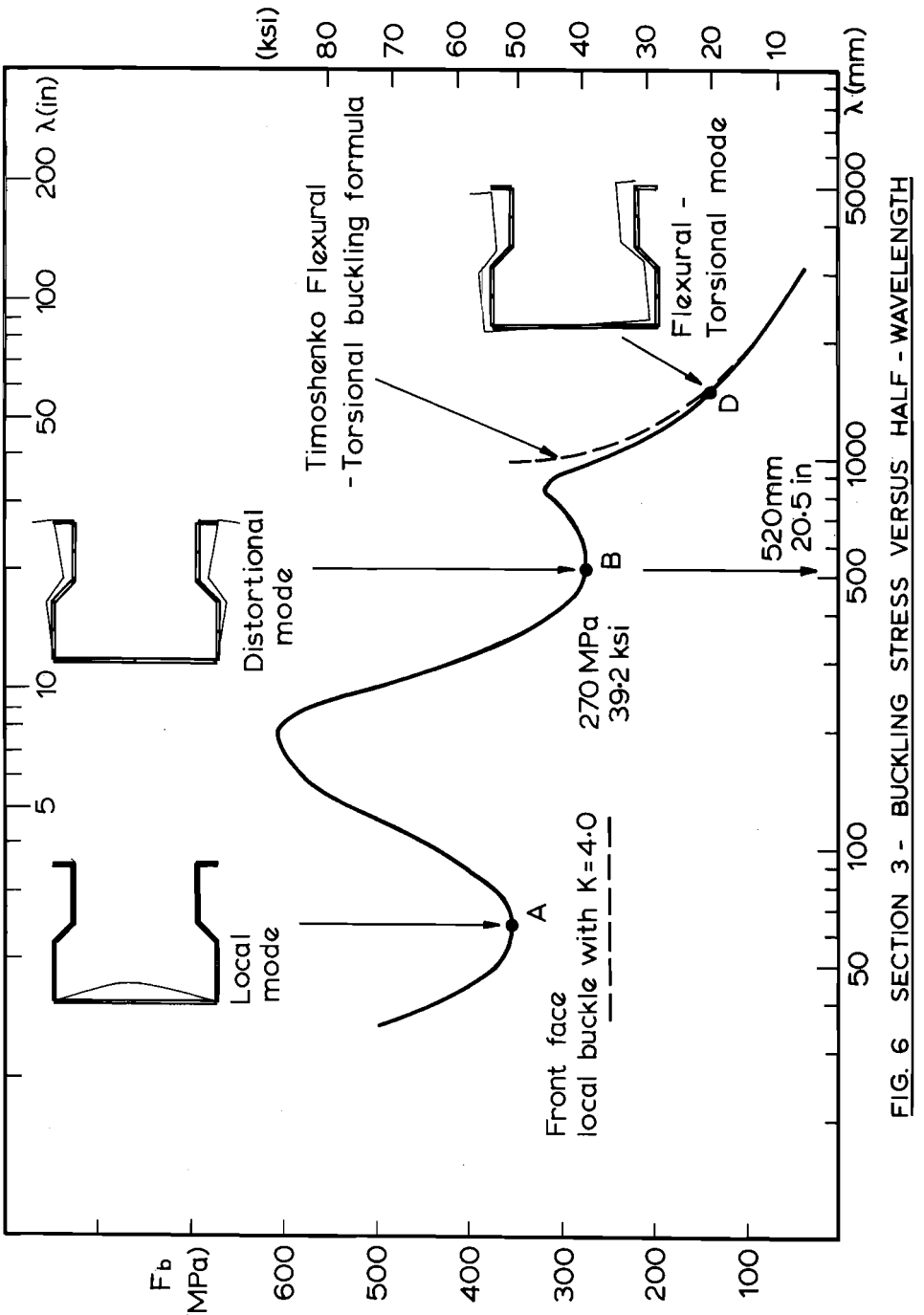

FIG. 6 SECTION 3 - BUCKLING STRESS VERSUS HALF-WAVELENGTH

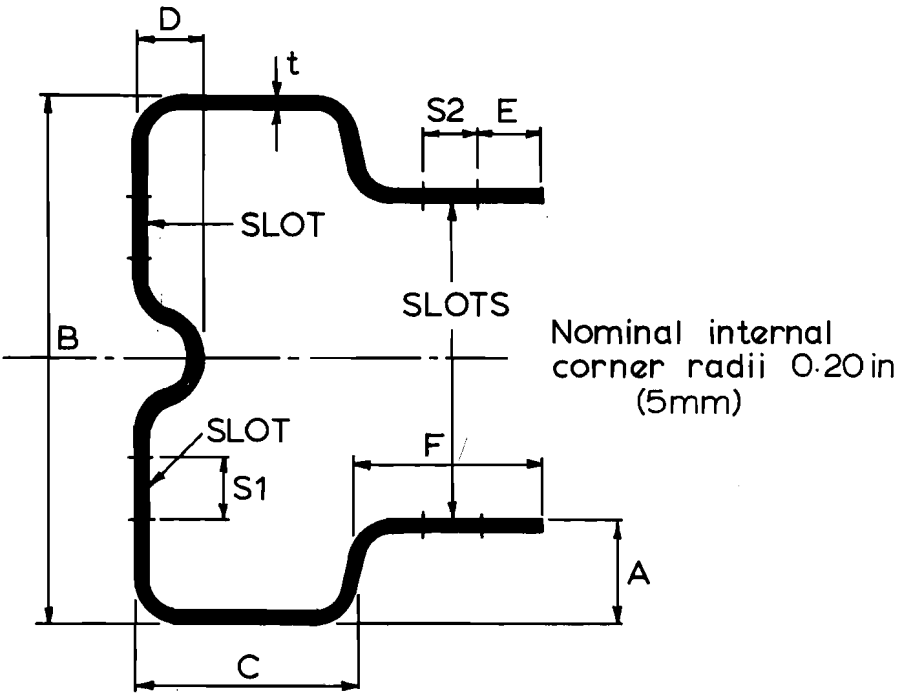

FIG. 7 SECTION NO: COOOI

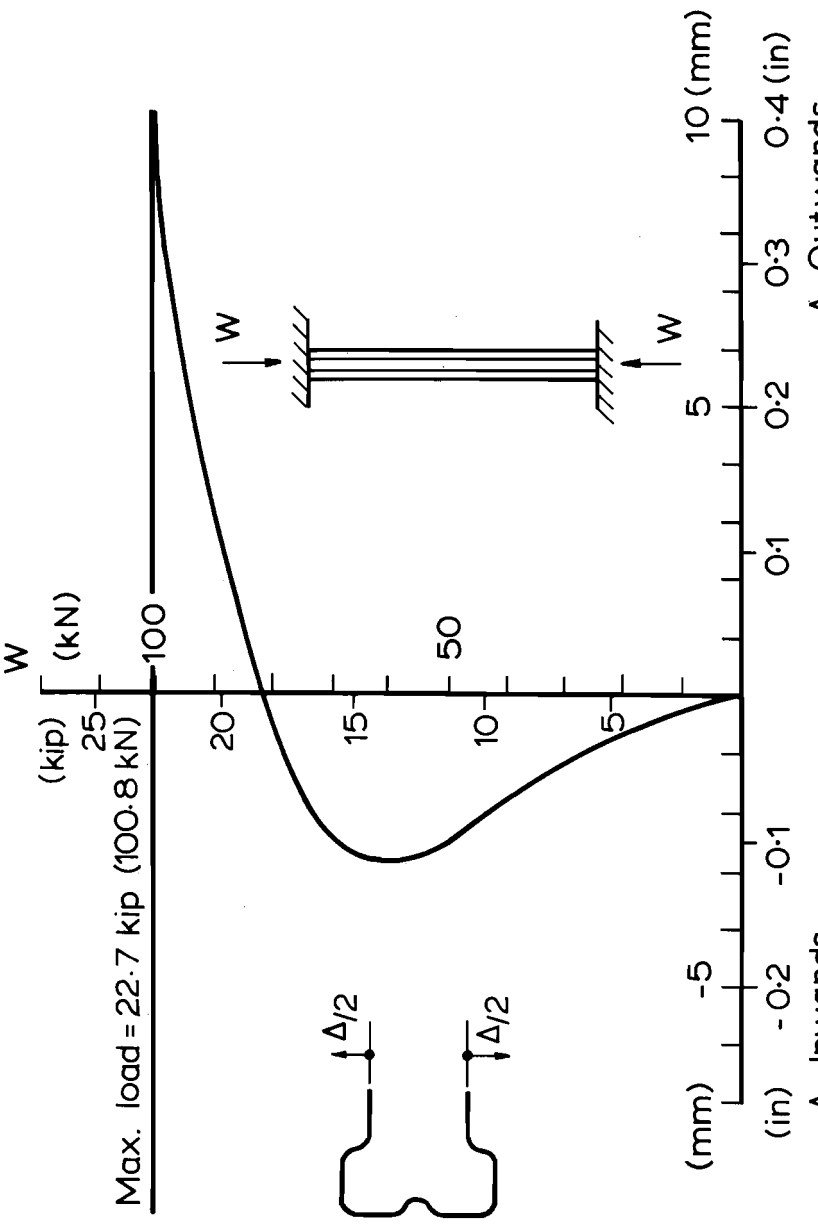

FIG. 8 LOAD VERSUS DISTORTIONAL DISPLACEMENT (Specimen D1)

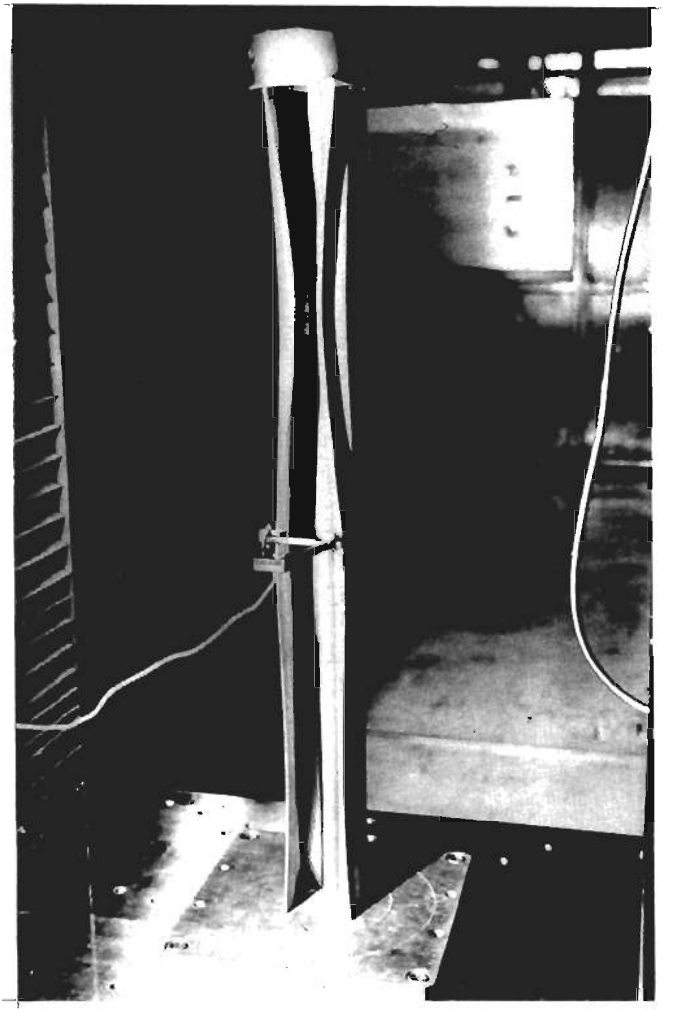

FIG. 9 DISTORTIONAL BUCKLING MODE OF SPECIMEN DI AT A LOAD OF 21·4 kips (95kN)

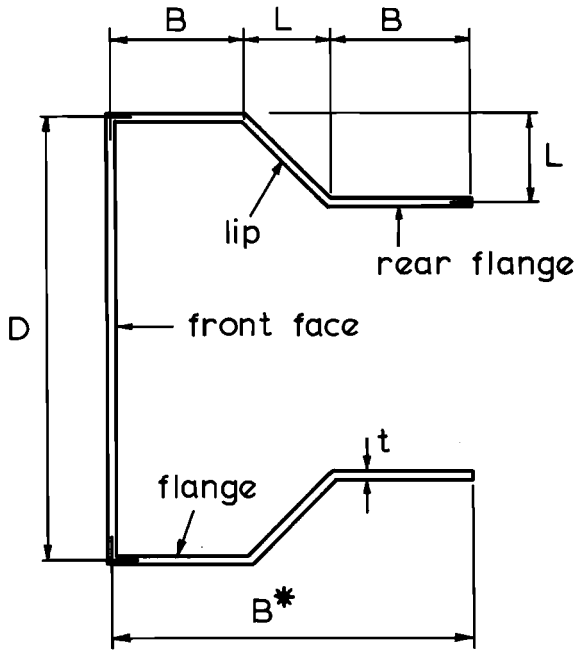

$$F_d = K_d \frac{\pi^2 E}{12(1-\nu^2)} \left(\frac{t}{B^*}\right)^2$$

FIG. 10 SECTION GEOMETRY FOR DESIGN CHART

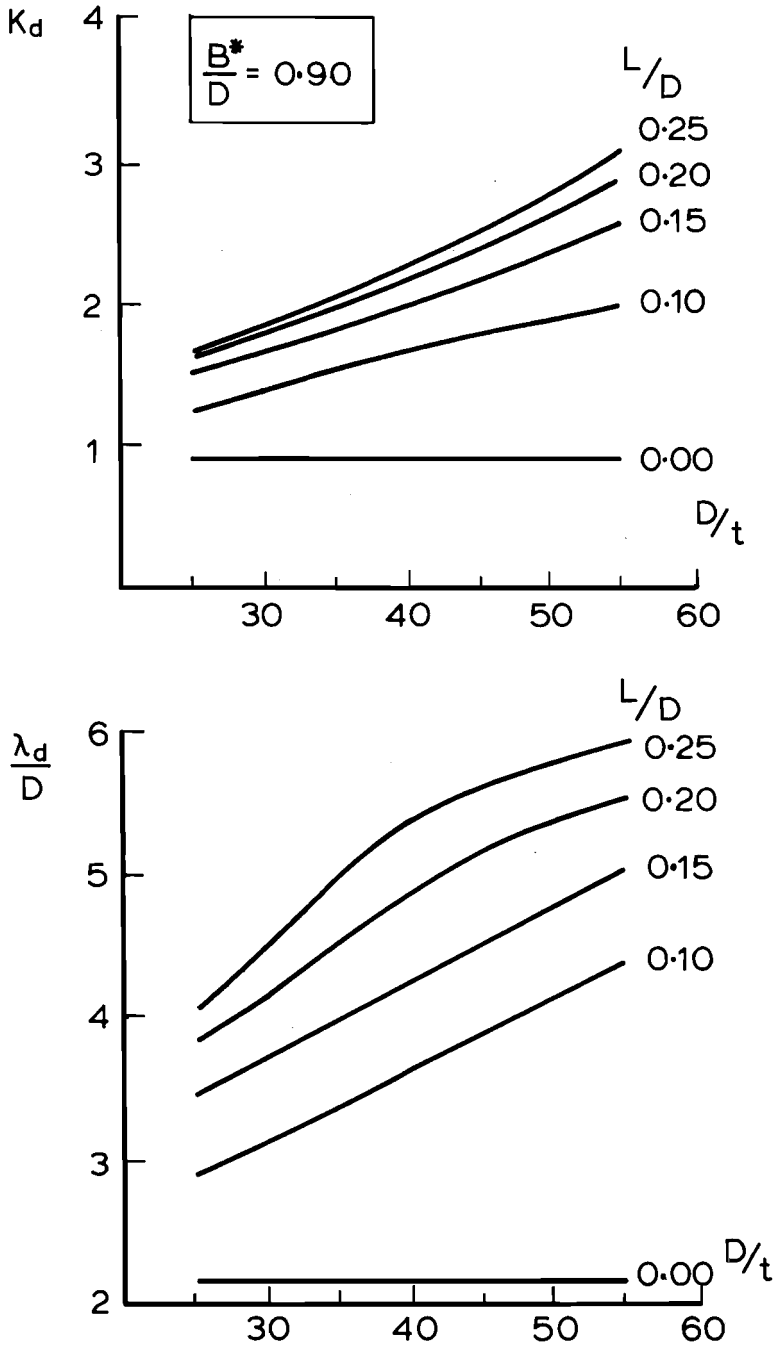

FIG. 11 DISTORTIONAL BUCKLING COEFFIENT (Kd) AND HALF - WAVELENGTH (λd)

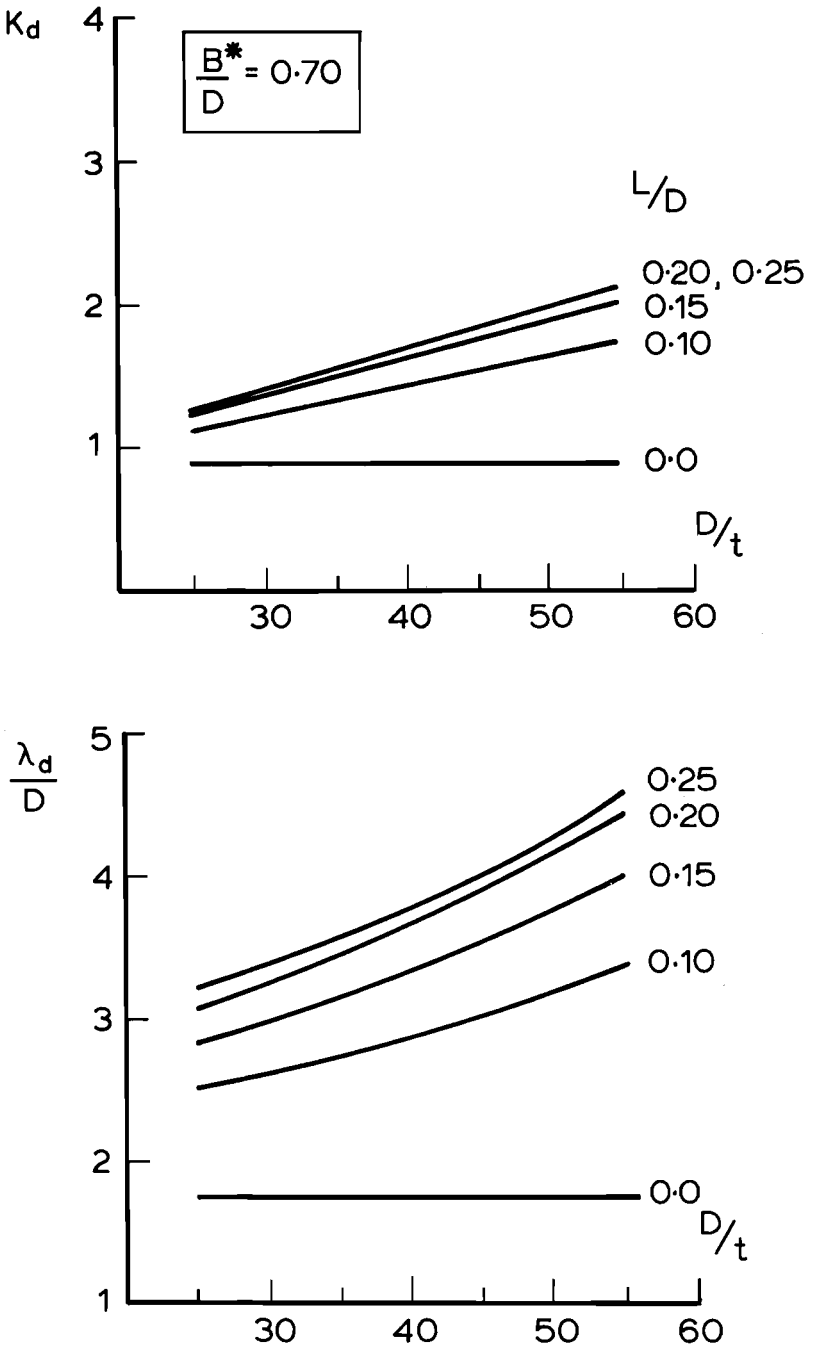

FIG. 12 DISTORTIONAL BUCKLING COEFFIENT (Kd) AND HALF-WAVELENGTH (λd)